

RSC Advances

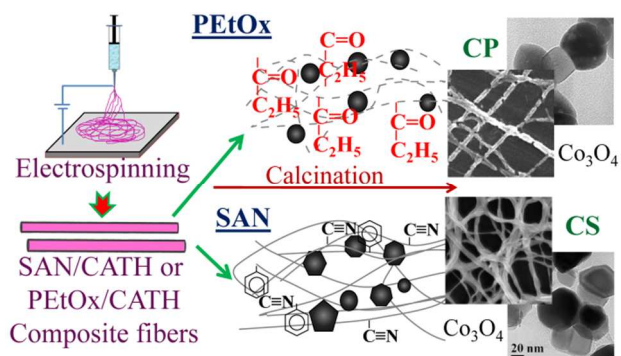


This is an *Accepted Manuscript*, which has been through the Royal Society of Chemistry peer review process and has been accepted for publication.

Accepted Manuscripts are published online shortly after acceptance, before technical editing, formatting and proof reading. Using this free service, authors can make their results available to the community, in citable form, before we publish the edited article. This *Accepted Manuscript* will be replaced by the edited, formatted and paginated article as soon as this is available.

You can find more information about *Accepted Manuscripts* in the [Information for Authors](#).

Please note that technical editing may introduce minor changes to the text and/or graphics, which may alter content. The journal's standard [Terms & Conditions](#) and the [Ethical guidelines](#) still apply. In no event shall the Royal Society of Chemistry be held responsible for any errors or omissions in this *Accepted Manuscript* or any consequences arising from the use of any information it contains.



Physico-chemical characteristics of cobalt oxide nanofibers were tailored by varying the sacrificial polymeric binder in sol-gel electrospinning.



A Comparative Study on the Physico-chemical Properties of Sol-Gel Electrospun Cobalt Oxide Nanofibres from Two Different Polymeric Binders

Received 00th January 20xx,
Accepted 00th January 20xx

DOI: 10.1039/x0xx00000x

www.rsc.org/

Gibin George and S. Anandhan*

In this study, two different sacrificial polymeric binders, namely poly(2-ethyl-2-oxazoline) (PEtOx) and poly(styrene-co-acrylonitrile) (SAN) along with cobalt acetate tetrahydrate (CATH), as the metal oxide precursor, were used for the fabrication of Co_3O_4 nanofibres through sol-gel electrospinning. It was observed that the degradation behaviour and physical properties of SAN and PEtOx influenced the structure, morphology and spectral properties of Co_3O_4 nanofibres, as the properties of nanofibres obtained from the aforementioned systems were compared with each other. The grain size, shape and the activation energies for grain growth of Co_3O_4 nanofibres obtained from these two polymeric systems were different. This difference in grain size and shape caused a difference in the optical band gap energies and the magnetic properties of the Co_3O_4 nanofibres. This study reveals that one can tailor the characteristics of cobalt oxide nanofibres by an appropriate selection of polymeric binders for sol-gel electrospinning.

Introduction

Metal oxide nanomaterials with different morphology and structures exhibit different functional properties. The characteristics of an oxide nanomaterial also depend on its synthetic route. The properties of an oxide material with a definite shape fabricated by a top down approach may not be the same as that of one prepared by a bottom up approach. This difference in properties with the fabrication route and the morphology opens up the huge potential of the oxide nanomaterials for a wide range of applications. Thousands of oxide nanomaterials with different morphologies and structures have been fabricated and their potential applications are exploited in detail. By the introduction of oxide nanomaterials, many traditional materials, which were once considered to be ideal for certain applications, have been replaced.¹ In many applications high aspect ratio nanomaterials are preferred over their low aspect ratio counterparts.

Electrospinning assisted sol-gel processing is the most feasible approach for the production of high aspect ratio ceramic oxide nanofibres in large scale.² In a typical sol-gel electrospinning, a spinnable sol (a mixture of polymer, solvent and precursor metal salt with adequate viscosity) is spun to nanosized composite fibres and these fibres are calcined above the degradation temperature of the organic part in the composite fibres.³ Myriads of oxide nanofibres have been

fabricated using electrospinning assisted sol-gel processing. A handful of organic polymers as binders have been used for the fabrication of these oxides. These are: poly(vinyl alcohol),^{4–6} poly(N-vinyl pyrrolidone),^{7–10} poly(vinyl acetate),^{11–12} poly(acrylonitrile),¹³ etc. But, there are other polymer-solvent systems, which can be used as sacrificial binders in sol-gel electrospinning process of ceramic nanofibres. These polymers may perform better than the already reported polymers for the fabrication of ceramic fibres. The morphological and structural properties of the obtained ceramic nanofibres determine the suitability of the polymer for such an application. A comparison detailing the properties of the ceramic oxide obtained from different polymer systems is necessary to understand the importance of various polymers in this synthetic process.

The role of polymers in sol-gel assisted electrospinning of ceramic nanofibres is to improve the spinnability of the metal-salt precursor sol. Also, polymers act as the structural element in transferring the morphology of the composite fibres to the ceramic fibres.¹⁴ Spinnability of some polymers is better than the others, but they may exhibit poor performance during the degradation and to transfer the morphological features of the composite fibres. In high temperature processing of oxide nanomaterials, the nature of the surrounding medium can greatly influence the properties of final ceramic oxide, since; at nanoscale a large number of atoms are present at the surface, which determines the property of the material under consideration. The defects in nanomaterials dictate their unique properties¹⁵ and the defects formation is influenced by the precursor used and its nature of degradation. Especially, in polymer assisted fabrication of ceramic nanofibres through electrospinning, the degradation behaviour and the degraded

Department of Metallurgical and Materials Engineering,
National Institute of Technology-Karnataka, Srinivas Nagar, Mangaluru-575025,
India. E-mail: anandtmg@gmail.com & anandhan@nitk.edu.in
Fax: +91-824-2474059; Tel: +91-824-2473762

*Electronic Supplementary Information (ESI) available: See
DOI: 10.1039/x0xx00000x

products of polymer can greatly influence the characteristics of the final metal oxide.¹⁴ Among the two modes of preparing the spinnable sol,³ polymer assisted fabrication is best suited for the scalable production.

This work is an attempt to understand the importance of the choice of polymers for the fabrication of Co₃O₄ nanofibres through sol-gel assisted electrospinning process. Cobalt oxide (Co₃O₄) nanofibres/nanomaterials exhibit multifunctional properties. Co₃O₄ based nanomaterials/nanofibres are suitable candidates for sensing¹⁶, heterogeneous catalysis¹⁷, oxygen and hydrogen evolution catalysts¹⁸, supercapacitors¹⁹, lithium-ion batteries²⁰ and as magnetic materials²¹.

Co₃O₄ nanofibres were fabricated using two sacrificial binders based on poly(2-ethyl-2-oxazoline) (PEtOx) and poly(styrene-co-acrylonitrile) (SAN). Since the degradation behaviour of the polymer used as binder can significantly affect the properties of the fibres, the scope of this work lies on optimizing the properties of ceramic nanofibres by the suitable selection of the polymer, and it is not just limited to that of electrospun ceramic nanofibres but also to the nanomaterials prepared by sol-gel technique. PEtOx is a water soluble polymer and SAN is an organo soluble one, the difference in the morphological, structural, magnetic and optical properties of the Co₃O₄ nanofibre mats obtained using the systems based on the aforementioned polymers were studied.

Experimental

PEtOx purchased from Alfa Aesar, Bangalore, India, SAN (Grade: Santron IMS 1000, acrylonitrile content: 30%, specific gravity: 1.07, viscosity average molecular weight (\overline{M}_v): 2.46×10^6 g mol⁻¹, melt flow index (MFI): 35 g/10 min at 220 °C under a load of 10 kg, ASTM D-1238) obtained from Bhansali polymers, Rajasthan, India, *N,N* dimethyl formamide (DMF) procured from SRL laboratory chemicals, Mumbai, India and cobalt acetate tetrahydrate (CATH) (assay > 99%) bought from High purity laboratory chemicals, Mumbai, India were used as the precursors for the fabrication of Co₃O₄ nanofibres.

The two spinnable sols with PEtOx and SAN as binders were prepared separately. PEtOx/CATH was prepared by dissolving 2g of PEtOx in 10 mL of distilled water, followed by the addition of 2g of CATH. Similarly, 2g of SAN was dissolved in 10 mL of DMF followed by the addition of 2g of CATH, to prepare the spinnable sol of SAN/CATH. Both the solutions were stirred vigorously for six hours to ensure the uniform mixing. The mixtures were stirred vigorously to ensure uniform mixing. Thus the spinnable sol was obtained.

These mixtures were loaded to a vertical electrospinning machine (E-spin nano, Chennai, India) using a 10 mL syringe attached with a hypodermic needle (inner diameter: 0.5 mm and outer diameter: 0.8 mm). While the high DC voltage was applied, the nanosized fibres were collected on the collector plate of the spinning unit. For PEtOx/CATH composite fibres, the applied voltage was 20 kV, flow rate was 300 μ L h⁻¹ and spinneret tip to collector distance was 25 cm. For SAN/CATH composite fibres, the applied voltage was 22 kV, flow rate was 1000 μ L h⁻¹ and the tip to collector distance was 17 cm. These

optimum processing conditions were chosen on the basis of fibre uniformity, a narrow diameter distribution and yield of the xerogel fibres obtained during the electrospinning process. These composite fibres were calcined above the degradation temperature of the organic phases of the composite fibres, which was in turn determined from thermogravimetric analysis (TGA) (EXSTAR 6000 TG/DTA 6300, Japan, under a nitrogen atmosphere at a heating rate of 10 K min⁻¹). The calcination was carried out under a controlled heating rate of 4 °C min⁻¹ in an air atmosphere followed by a dwell period of 2 h using a programmable furnace (Indfurr, Chennai, India). Thus obtained Co₃O₄ nanofibres are represented with the codes as in Table 1.

Table 1 Sample description

Sample code	Description
CP500	Co ₃ O ₄ nanofibres obtained using PEtOx as sacrificial binder at 500 °C
CP600	Co ₃ O ₄ nanofibres obtained using PEtOx as sacrificial binder at 600 °C
CS500	Co ₃ O ₄ nanofibres obtained using SAN as sacrificial binder at 500 °C
CS600	Co ₃ O ₄ nanofibres obtained using SAN as sacrificial binder at 600 °C

To compare the morphological and structural properties of the fibres, the fibres were characterized using scanning electron microscopy (SEM) (JEOL JSM-6380LA, Japan, the samples were gold sputtered using JFC 1600 autofine coater, JEOL, Japan), energy dispersive X-ray spectroscopy (EDS) (Link ISIS-300 Micro-analytical System, Oxford Instruments, UK), transmission electron microscopy (JE-200 JEOL, Japan), Fourier transform infrared (FTIR) spectroscopy (Jasco FTIR-4200, Japan, in transmission mode by KBr pellet method, recorded with a resolution of 1 cm⁻¹ and an average of 32 scans), Raman spectroscopy (inVia, Renishaw, UK, using an Argon ion laser source with a power of 100 mW and a wavelength of 514 nm) and wide angle X-ray diffraction (JEOL X-ray diffractometer, DX-GE-2P, Japan, scanning rate was 0.5° min⁻¹, using CuK α radiation). The optical properties of the Co₃O₄ fibres were analyzed by UV-Vis-NIR spectroscopy (Varian, Cary 5000 UV-Vis-NIR, USA, in the wavelength range of 215-2400 nm). The room temperature magnetic properties of Co₃O₄ nanofibres were studied using a vibrating sample magnetometer (7404, Lake Shore Cryotronics, Inc., USA). The XPS analysis [Axis 165, X-ray Photoelectron Spectrometer, Kratos Analytical, UK, using monochromated Al K α radiation (15 keV) for excitation] of two representative samples of Co₃O₄ nanofibres was done to ensure the complete degradation of organic part present in the nanofibres.

Results and discussion

The minimum calcination temperature of the composite nanofibres was determined from the TG analysis of the fibres (Fig. 1).

The PEtOx/CATH fibres degraded at a lower temperature as compared with SAN/CATH fibres. In the TGA curves, the elimination of water took place at 100 °C, followed by the removal of acetic acid from CATH. This acetic acid can accelerate the degradation of the polymers. In PEtOx, the degradation takes place by the by random chain scission of the polymer back bone followed by the elimination of side chains,²² whereas in SAN, side groups are eliminated first, followed by the degradation of backbone.²³ The mechanisms of degradation of both the polymers are opposite to each other. In the case of PEtOx protonated monomers and oligomers are evolved as the degradation commences, whereas in SAN nitrile groups are released first, followed by the elimination of oligomers and small aromatic compounds. An overall conversion process of PEtOx/CATH and SAN/CATH composite fibres to the respective Co₃O₄ nanofibres during calcination is shown in Scheme 1.

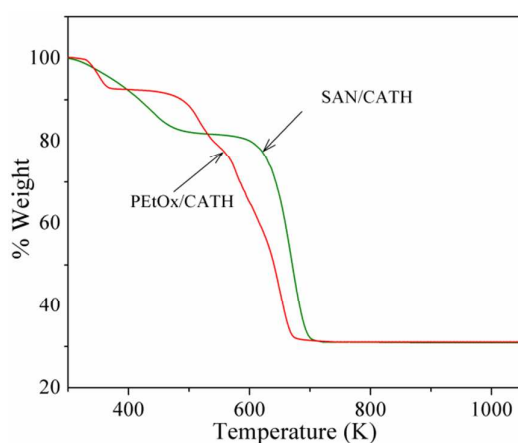
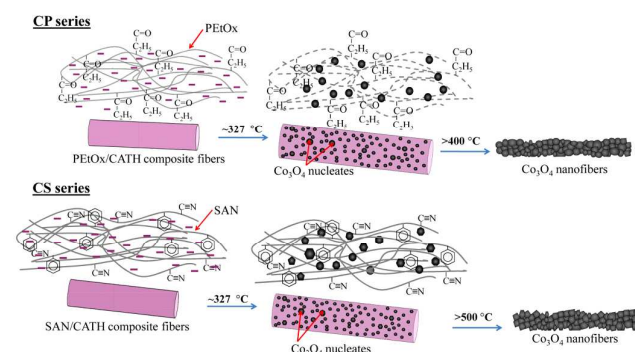


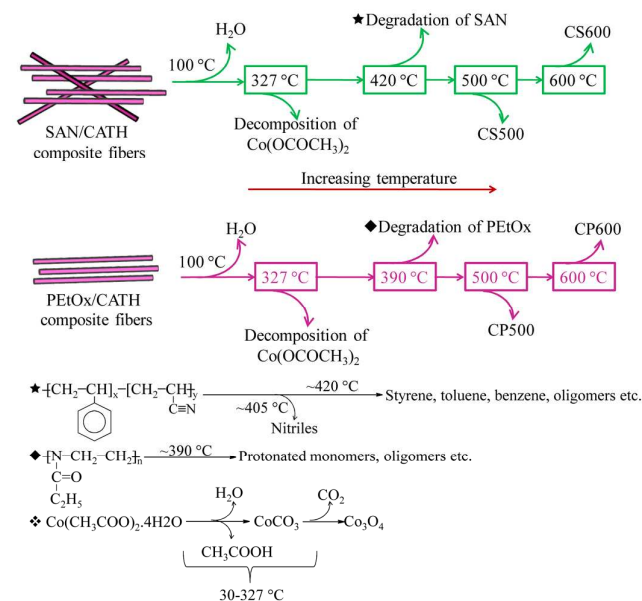
Fig. 1 TGA curves of SAN/CATH and PEtOx/CATH composite fibres

The char in TG analysis represents Co₃O₄ nanofibres formed during calcination. The weight of the char is comparable with the Co₃O₄ yield from CATH.

The SEM micrographs of PEtOx/CATH and SAN/CATH composite nanofibres are shown in Fig. 2a & 2b, respectively. The smooth fibres spun on the collector plates are randomly oriented. A low average fibre diameter is observed in the case of PEtOx/CATH composite fibres, which is 186 nm, whereas in the case of SAN/CATH fibres it is 274 nm. These morphological features of the composite fibres changed during the calcination process. The average diameter of the obtained Co₃O₄ nanofibres is less compared with that of the composite fibres. This reduction is large in the case of SAN/CATH system than the PEtOx/CATH system. The reduction in fibre diameter with calcination temperatures is due to the elimination of the organic part from the composite fibres. The aspect ratio of the nanofibres can be more than tens of thousands as per literature.¹⁵ Aspect ratio of electrospun nanofibres is very difficult to measure as they deposit randomly during their electrospinning.



Scheme 2 Influence of polymeric binders on the nucleation of Co₃O₄ nanofibres



Scheme 1 Overall conversion process of composite fibres during calcination

In CP500 and CP600, the early decomposition of PEtOx (~390 °C) initiated from the backbone²² and the inherently brittle nature of Co₃O₄ resulted in the formation of fibres with rugged morphology. In the case of SAN/CATH system, the stability of SAN at a slightly higher temperature and the ability of styrene groups as structural elements, help to maintain the smooth morphology in calcined CS500 and CS600 nanofibres. As the fibrous morphology of the obtained Co₃O₄ was confirmed from the SEM analysis, the finer details of the Co₃O₄ grains, which compose the fibres, were analyzed using TEM after ultrasonication of the fibres in ethanol. The morphology of the fibres can be destroyed during ultrasonic treatment, as evident from the TEM image of the single CS600 series fibre and SEM image of the sonicated CP600 series fibres (†ESI, Fig. S1a&b). The TEM images (Fig. 3) show that the Co₃O₄ nanofibres are composed of many nanosized crystallites. The SAED pattern in the inset can be indexed to typical Co₃O₄ and the lattice fringes correspond to that of Co₃O₄. The grain size is increased as the calcination temperature is increased. The grain sizes of CS series Co₃O₄ nanofibres are bigger than the respective CP series fibres. In CS series nanofibres, many grains have hard edges compared with those of the respective CP

series nanofibres. This can be due to the presence of SAN at the nucleation and growth temperature of Co_3O_4 grains to guide the growth in certain direction,³⁰ which happens at $\sim 327^\circ\text{C}$. In CP series nanofibres, the degradation of PETox takes place straight away after the formation of Co_3O_4 nucleates from CATH, whereas in the case of SAN, it is assumed that the degradation starts as the nucleation progresses; therefore, the polymer may be available for the controlled growth of the crystals. A mechanism of nucleation during Co_3O_4 nanofibre formation as SAN and PETox are used as sacrificial binders is shown in Scheme 2.

The SEM–EDS results of the Co_3O_4 nanofibres obtained from the two types of composite fibres are presented in Table 2. In Co_3O_4 nanofibres CP500 and CS500, which are obtained at lower calcination temperature (500°C), the deviation in

stoichiometry is large as compared with the perfect stoichiometry of Co_3O_4 . For the fibres, CP600 and CS600, the composition is approaching that of a perfect stoichiometric ratio of cobalt and oxygen in Co_3O_4 . The difference in composition is not affected by the nature of degradation of the sacrificial polymeric binders to a large extent, because the structure of Co_3O_4 itself has excess oxygen in it. To be precise, in Co_3O_4 the atomic ratio of oxygen is higher than that of cobalt, which can limit the amount of oxygen molecules that can be adsorbed on to the lattice sites of Co_3O_4 during its formation at high temperatures. Therefore, it can be concluded that even at high temperature the surrounding oxygen doesn't significantly influence the stoichiometry of Co_3O_4 nanofibres.

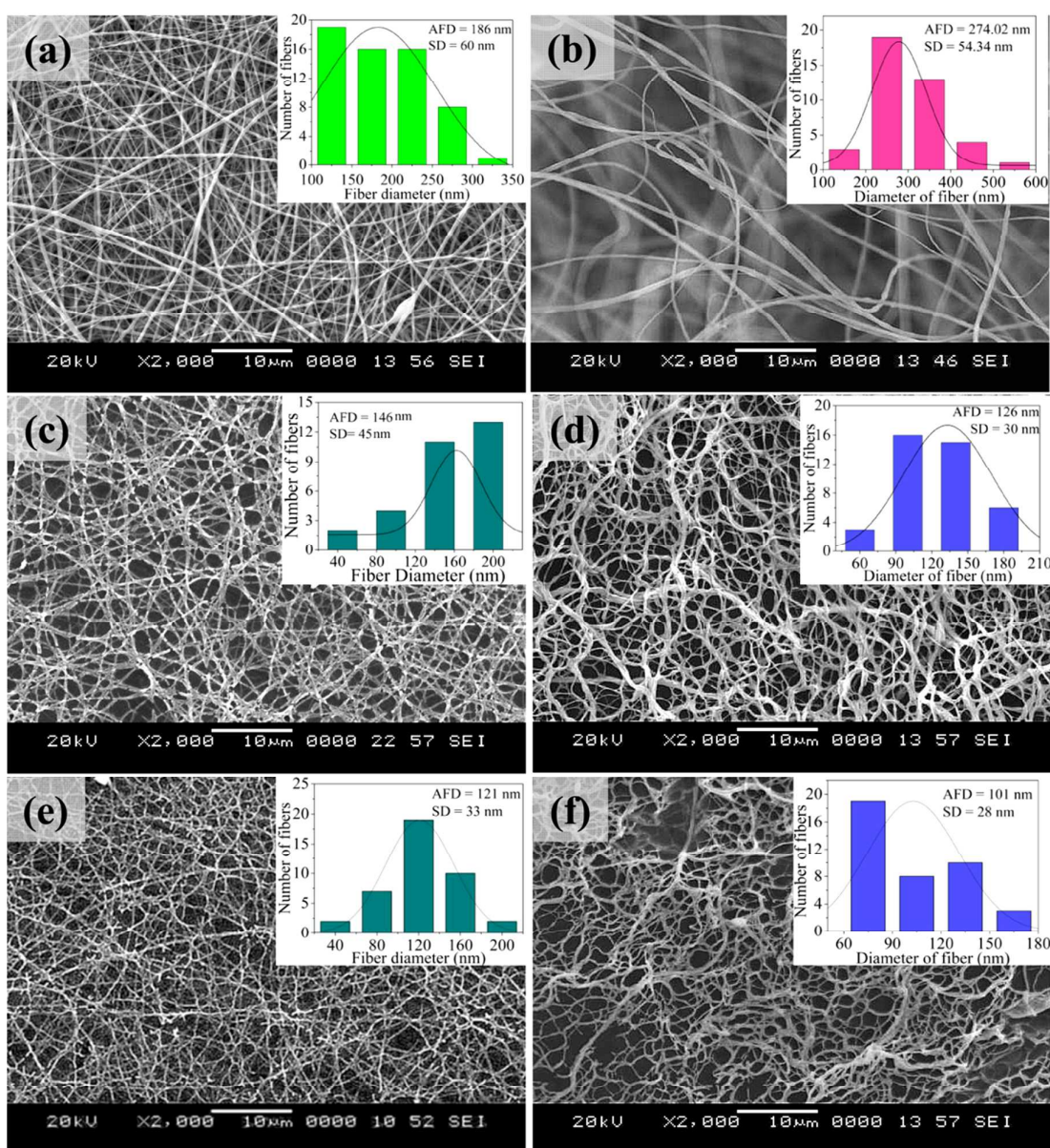


Fig. 2 SEM micrographs of (a) PETox/CATH composite nanofibres, (b) SAN/CATH composite nanofibres, (c) CP500, (d) CS500, (e) CP600 and (f) CS600. Inset shows the histogram, average fibre diameter (AFD) and standard deviation of fibre diameter (SD).

Table 2 EDS results of CP and CS fibre series

Sample code	Mass percentage (%)				Atomic percentage (%)			
	Actual		Theoretical		Actual		Theoretical	
	Cobalt	Oxygen	Cobalt	Oxygen	Cobalt	Oxygen	Cobalt	Oxygen
CP500	67.93	32.07			36.51	63.49		
CP600	71.28	28.72	73.42	26.58	40.94	59.06	42.86	57.14
CS500	67.97	32.03			36.56	63.44		
CS600	72.40	27.60			41.59	57.07		

The FTIR spectra of the PETox/CATH and SAN/CATH composite fibres and the corresponding Co_3O_4 nanofibres after calcination are shown in Fig. 4. In the spectra of the calcined fibres, the peak representing that of the organic matter are completely eliminated, indicating the degradation of the organic matter from the composite fibres. The FTIR spectral peaks of the calcined fibres manifest the typical cobalt oxide with spinel structure. The two absorption peaks at 573 cm^{-1} and 667 cm^{-1} , which originate from the stretching vibrations of the

metal-oxygen bond, confirm the formation of Co_3O_4 . The band at 573 cm^{-1} is distinguished as OB_3 (B denotes the Co^{3+} in the octahedral site) vibration and the band at 667 cm^{-1} is due to the ABO_3 (A denotes the Co^{2+} in the tetrahedral site) vibration in the spinel lattice.³¹ The higher intensity of the peaks in the spectra of CS500 nanofibres than CP500 fibres is due to the larger grain sizes in these fibre systems. The grain sizes were measured for 50 grains with definite shapes (aspect ratio ≈ 1).

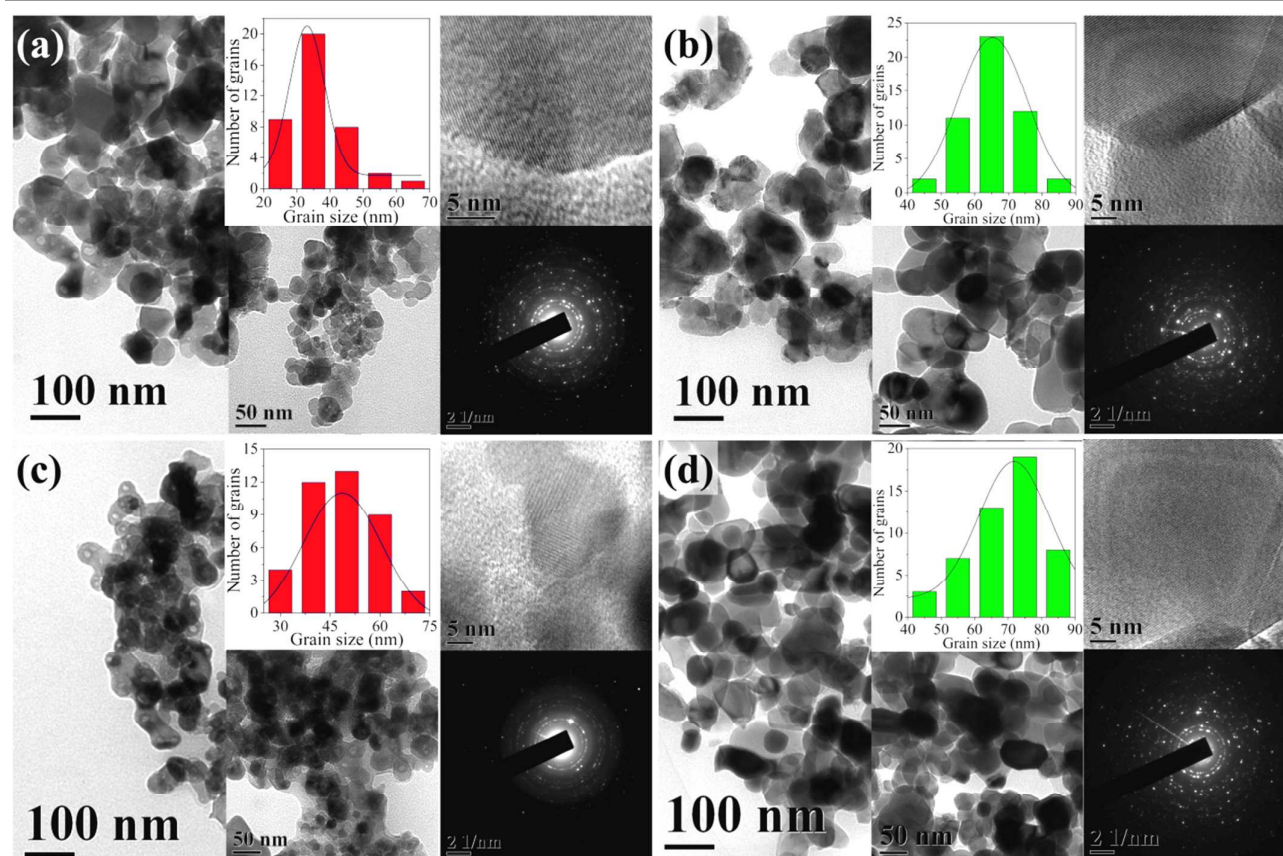


Fig. 3 TEM images of the grains along with the histograms, high resolution images and SAED patterns of (a) CP500, (b) CS500, (c) CP600 and (d) CP600.

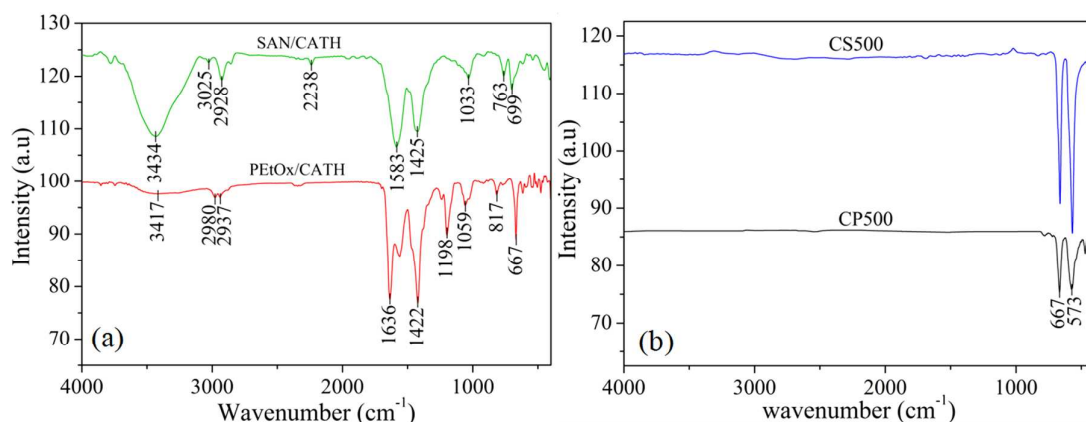


Fig. 4 FTIR spectra of (a) SAN/CATH and PETOx/CATH composite fibres and (b) CS500 and CP500 fibres.

The Raman spectra of the CP500 and CS500 nanofibres obtained from the two different polymer based systems are shown in Fig. 5.

Co_3O_4 with spinel structure and O_h symmetry, the vibrational modes are,³²

$$\Gamma = A_{1g} + E_g + 3F_{2g} + 5F_{1u} + 2A_{2u} + 2E_u + 2F_{2u} \quad (1)$$

A_{1g} , E_g , and the three F_{2g} modes are Raman active. The peak at 688 cm^{-1} corresponds to A_{1g} , that at 479 cm^{-1} corresponds to E_g and those at 191, 520 and 616 cm^{-1} correspond to the three F_{2g} modes of vibrations, respectively. The intensity of the Raman peaks increases as a function of the scattering efficiency of a material, which will be ultimately determined by the grains size of the materials. In the present study, the intense peaks of CS500 nanofibres are due to their larger grains than those composing CP500 fibres.

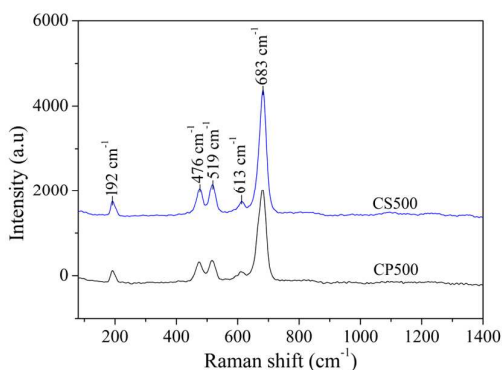


Fig. 5 Raman Spectra of CS500 and CP500 fibres

The XRD patterns of the Co_3O_4 nanofibres calcined at $500 \text{ }^\circ\text{C}$ using PETOx and SAN as the sacrificial binders are shown in Fig. 6. The XRD patterns of the Co_3O_4 nanofibres were compared with the JCPDS-42-1467 standard line diffraction pattern as in Fig. 6 and the peaks are matching with that of the standard Co_3O_4 sample. The grain sizes of the Co_3O_4 nanofibres were calculated by Sherrer formula (Eqn. 2) using the full width at half maximum (FWHM) for the peak corresponding to the (311) plane.

$$\beta = \frac{k\lambda}{D\cos\theta} \quad (2)$$

Where, β is the full width at half maximum, k is a constant whose value is 0.9, λ is the wavelength of X-rays used, θ is the position of the peak and D is the grain size.

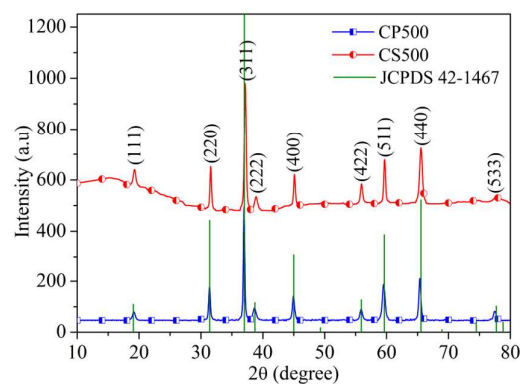


Fig. 6 XRD pattern of CS500 and CP500 nanofibres

Table 3 Grain sizes and activation energies of grain growth of Co_3O_4 nanofibres

Sample code	Grain size (nm)	Activation energy ($\text{kJ}\cdot\text{mol}^{-1}$)
CP500	24.1	16.3
CP600	32.2	
CS500	31.4	11.2
CS600	38.7	

The grain sizes obtained using XRD are lower than that obtained from TEM analysis, because of the polycrystalline nature of the grains composing the fibres, as observed in the TEM results. The grain size of the two sets of Co_3O_4 nanofibre obtained at 500 and $600 \text{ }^\circ\text{C}$ are presented in Table 3. The grain sizes increase as a function of calcination temperature. It is due to the temperature assisted diffusion process. The grain growth associated with temperature is substantiated with Arrhenius equation,²⁷

$$D = A \exp\left(\frac{-E_a}{RT}\right) \quad (3)$$

Where, D is the grain size, E_a is the activation energy, T is the temperature of calcination and R is the universal gas constant, $8.314 \text{ J mol}^{-1} \text{ K}^{-1}$.

The average activation energy for the grain growth in the Co_3O_4 fibres from the two polymeric systems was determined by solving Eqn. 3 for grain sizes corresponding to two subsequent temperatures. The reduction in activation energy of grain growth of the Co_3O_4 nanofibres obtained from SAN/CATH composite fibres resulted in larger grains as compared with those obtained from PETox/CATH composite fibres. The degradation temperature of the organic matter in the composite fibres influences grain growth and the activation energy in nanofibres. If the degradation temperature of the polymer is high, the carbon rich residue remains in the system during the formation of Co_3O_4 , which in turn can act as a medium for ionic transport.²⁸ This factor can reduce the effort for the ionic/atom movements and thereby the activation energy too can be less, which can increase the chances of rapid growth of the nucleates initially. Therefore, the reduction in activation energy for grain size enhancement in Co_3O_4 nanofibres prepared from SAN/CATH system is due to the high degradation temperature and the nature of degradation of SAN.

An appreciable difference in the room temperature magnetic properties of the Co_3O_4 nanofibres obtained using two sacrificial polymeric binders was observed (Fig. 7). Both types of nanofibres are ferromagnetic in nature, but the size of the hysteresis loop of CS500 is larger than that of CP500. In general, in oxygen rich oxide materials, cationic vacancies are dominant, which can induce the ferromagnetic behaviour in oxide material based on the ionization of the vacancy.²⁹ The magnetic parameter values of the Co_3O_4 nanofibres are shown in Table 4.

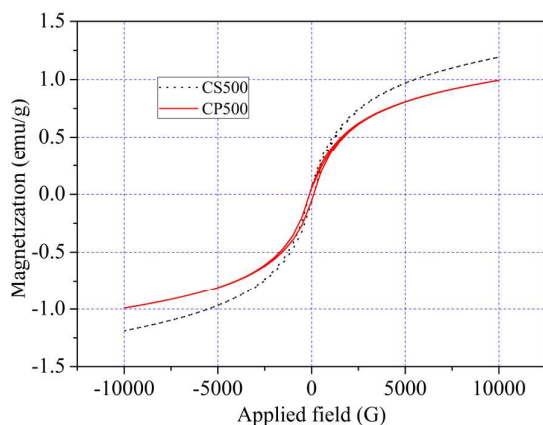


Fig. 7 Room temperature magnetization-demagnetization behaviours of two representative types of Co_3O_4 nanofibres

Co_3O_4 as a bulk material is antiferromagnetic, whereas, its nanofibres exhibit weak ferromagnetic behaviour. The transition from antiferromagnetic to ferromagnetic behaviour

can be ascribed to the surface spins and the unpaired spins arising from the distortions in the crystals.²³ The decrease in magnetization with the calcination temperature, i.e., CP500 to CP600 and CS500 to CS600, can be attributed to the splitting of magnetic domain in the crystals with sizes above the critical single domain size. Therefore, the single-domain becomes multidomains, and the formation of domain walls will result in the decreased magnetization.^{31,32} The large hysteresis loop of CS500 can be due to the bigger grains in them than CP500. Due to the bigger grains, the magnetic domains can have larger area, which can ultimately lead to increased magnetic property.

Diffuse reflectance UV-Vis-NIR absorption spectra of Co_3O_4 nanofibres obtained from the two polymer systems are shown in Fig. 8. The grain size of the fibres controls the absorbance spectra due to the quantum confinement. In UV-Vis-NIR spectra, peaks corresponding to typical Co_3O_4 transitions are observed; these are: crystal field ${}^4A_2(F) \rightarrow {}^4T_1(F)$ transitions at 1460 nm, an "intervalence" charge-transfer $\text{Co}^{2+} \rightarrow \text{Co}^{3+}$ representing an internal oxidation-reduction process at 1220 nm, and ligand-metal charge transfer events $\text{O}^{2-} \rightarrow \text{Co}^{3+}$ and $\text{O}^{2-} \rightarrow \text{Co}^{2+}$ at 657 nm and 2788 nm, respectively.³³

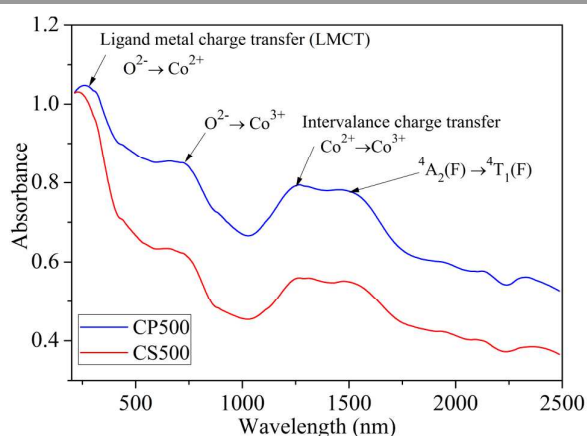


Fig. 8 UV-Vis-NIR spectra of two representative Co_3O_4 nanofibres

Since Co_3O_4 has a spinel structure, it has two band gap energies corresponding to the two oxidation states of cobalt, Co^{3+} and Co^{2+} .³⁴ The optical band gap can be obtained using the equation,³⁵

$$(\alpha h\nu)^2 \propto (h\nu - E_g) \quad (4)$$

Where, α is the absorption coefficient, $h\nu$ is the photon energy, E_g is the band gap, and n is either 1/2 for an indirect transition or 2 for a direct transition. The band gap energy was calculated by finding the x-intercept of the linear part in the plot $(\alpha h\nu)^2$ vs $h\nu$.

Table 4 Room temperature magnetic properties, band gap energy and surface area of Co_3O_4 nanofibres obtained from two series.

Sample code	Remanence (emu/g)	Coercivity (G)	Band gap energy (eV)		Surface area (m^2/g)
			B1	B2	
CP500	0.061	89.7	1.40	2.81	14.19
CP600	0.049	84.8	1.46	2.82	8.37
CS500	0.0658	91.4	1.27	2.72	15.65
CS600	0.050	91.5	1.35	2.83	7.16

With the change in the polymer systems used for obtaining Co_3O_4 nanofibres, differences in optical band gap energies are observed and similar changes are observed within each set as the calcination temperature is higher. This difference is due to the deviation from the stoichiometric ratio of cobalt and oxygen in the fibres when either the polymeric binder or the calcination temperature is changed. Richness in oxygen narrows down the band gap energy.³⁶ The band gap energies of the Co_3O_4 fibres are presented in Table 4.

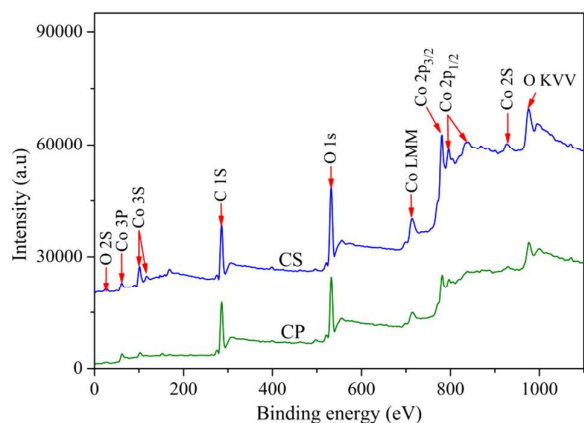


Fig. 9 Wide scan XP spectra of Co_3O_4 nanofibres obtained from the two different binders

In the wide angle XP spectra (Fig. 9) of CP and CS series, no appreciable difference is observed. The major peaks corresponding to Co 3p, Co 3s, C 1s, O 1s, Co 2p, Co 2s etc. are observed in both the spectra.

The two significant XP spectral peaks of Co 2p represent the split spin-orbit components Co $2p_{3/2}$ at ~ 780 eV and Co $2p_{1/2}$ at ~ 795 eV (Fig. 10), respectively. An energy separation of 15 eV was observed between Co ($2p_{3/2}$) and Co ($2p_{1/2}$) peaks, which is observed for a typical Co_3O_4 material.³⁷ The satellite peaks corresponding to Co^{2+} and Co^{3+} oxidation states of Co_3O_4 are also observed as expected and the asymmetry in the peaks is due to the existence of Co^{2+} in the tetrahedral sites and Co^{3+} in the octahedral sites of Co_3O_4 . While the comparison made among the C 2p spectra of CP and CS series nanofibres, there is a deviation in the core peak positions, which is attributed to the charge transfer from the metal ion to oxygen.

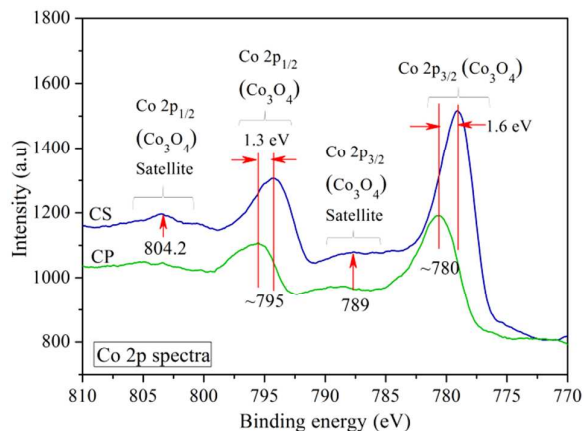


Fig. 10 Co 2p XP spectra of Co_3O_4 nanofibres obtained from the two different binders

In the present study, the binding energy of the CP series Co_3O_4 nanofibres are closely matching with that of a single crystal Co_3O_4 reported elsewhere,³⁸ whereas it is shifted for CS series Co_3O_4 . The XPS spectra are extremely sensitive to the stoichiometry and order of the surface;³⁹ also, atoms with higher oxidation state have higher binding energies due to the extra columbic interaction between the photo-emitted electron and the ion core.⁴⁰ The peak positions of CP series have an origin of Co^{3+} oxidation state, whereas it is Co^{2+} in CS series. Therefore, this shift in peak in CS series fibres can be correlated either to the large number of surface defects due to which Co^{3+} is reduced to Co^{2+} in the O position⁴¹ or the preferential growth of Co_3O_4 grains in the directions, which exploit Co^{2+} ions at the surface, i.e., (111) direction.⁴² A similar shift is observed in the O 1s Spectra also, which confirms the difference in stoichiometry in the fibres.

Conclusions

In summary, Co_3O_4 nanofibres were obtained from sols based on two polymeric binders and their structural, optical and magnetic properties were evaluated. The stability of SAN at high temperature improved the morphological features of CS series than CP series Co_3O_4 nanofibres. Larger grains were observed in Co_3O_4 nanofibres obtained from SAN/CATH fibres than that obtained from PETox/CATH fibres, which is due to the reduction in the activation energy for the grain growth in the former. The stoichiometric defects in Co_3O_4 fibres induced a ferromagnetic behaviour at room temperature and the size of the hysteresis loops was dependent on grain size. A difference in the optical band gap energy of the Co_3O_4 nanofibres were observed for fibres obtained from each polymeric binder as well the calcination temperatures used in the present study. Therefore, by this study it is concluded that by the appropriate selection of the polymeric binder in sol-gel electrospinning, and the calcination temperature one can customize the structural, electronic and magnetic properties of the Co_3O_4 nanofibres.

Acknowledgements

G.G. would like to thank the dept. of Metallurgical and Materials Engg., National Institute of Technology of Karnataka for a research fellowship. Authors would like to thank Mr. S. Varadharaja Perumal, CeNSE, IISc, Bangalore for the XPS studies. CIF, Pondicherry University, India is acknowledged for its kind assistance in Raman spectroscopy of the samples. The authors are very grateful STIC, Cochin, India, for the UV-Vis-NIR analysis of the samples.

References

- W. J. Stark, P. R. Stoessel, W. Wohlleben and A. Hafner, *Chem. Soc. Rev.*, 2015. Doi:10.1039/C4CS00362D.
- H. Wu, W. Pan, D. Lin and H. Li, *J. Adv. Ceram.*, 2012, **1**, 2–23.
- Y. Dai, W. Liu, E. Formo, Y. Sun and Y. Xia, *Polym. Adv. Technol.*, 2011, **22**, 326–338.
- S. K. Lim, S.-H. Hwang, D. Chang and S. Kim, *Sens. Actuators, B*, 2010, **149**, 28–33.
- S.-W. Choi, J. Y. Park and S. S. Kim, *Chem. Eng. J.*, 2011, **172**, 550–556.
- J. Y. Park and S. S. Kim, *J. Am. Ceram. Soc.*, 2009, **92**, 1691–1694.
- S. Chaudhari and M. Srinivasan, *J. Mater. Chem.*, 2012, **22**, 23049–23056.
- W. Zheng, X. Lu, W. Wang, Z. Li, H. Zhang, Y. Wang, Z. Wang and C. Wang, *Sens. Actuators, B*, 2009, **142**, 61–65.
- A.-M. Azad, *Mater. Sci. Eng., A*, 2006, **435–436**, 468–473.
- W. Nuansing, S. Ninmuang, W. Jarernboon, S. Maensiri and S. Seraphin, *Mater. Sci. Eng., B*, 2006, **131**, 147–155.
- S. J. Doh, C. Kim, S. G. Lee, S. J. Lee and H. Kim, *J. Hazard. Mater.*, 2008, **154**, 118–127.
- S.-W. Choi, J. Zhang, K. Akash and S. S. Kim, *Sens. Actuators, B*, 2012, **169**, 54–60.
- S.-J. Park, N. A. Barakat, K.-U. Jeong and H.-Y. Kim, *Polym. Int.*, 2011, **60**, 322–326.
- G. George and S. Anandhan, *Mater. Sci. Semicond. Process.*, 2015, **32**, 40–48.
- M. A. Carpenter, S. Mathur and A. Kolmakov, *Metal Oxide Nanomaterials for Chemical Sensors*, Springer Science & Business Media, New York, 2012.
- Y. Ding, Y. Wang, L. Su, M. Bellagamba, H. Zhang and Y. Lei, *Biosens. Bioelectron.*, 2010, **26**, 542–548.
- D. Zhang, Q. Xie, A. Chen, M. Wang, S. Li, X. Zhang, G. Han, A. Ying, J. Gong and Z. Tong, *Solid State Ionics*, 2010, **181**, 1462–1465.
- G. George, L. Elias, A. C. Hegde and S. Anandhan, *RSC Adv.*, 2015, **5**, 40940–40949.
- X. Lu, X. Huang, S. Xie, T. Zhai, C. Wang, P. Zhang, M. Yu, W. Li, C. Liang and Y. Tong, *J. Mater. Chem.*, 2012, **22**, 13357–13364.
- O. C. Compton, A. Abouimrane, Z. An, M. J. Palmeri, L. C. Brinson, K. Amine and S. T. Nguyen, *small*, 2012, **8**, 1110–1116.
- Y. Koseoglu, F. Kurtulus, H. Kockar, H. Guler, O. Karaagac, S. Kazan and B. Aktas, *J. Supercond. Nov. Magn.*, 2012, **25**, 2783–2787.
- N. Atilkan, Y. Nur, J. Hacaloglu and H. Schlaad, *Macromol. Chem. Phys.*, 2012, **213**, 945–951.
- T. J. Xue and C. A. Wilkie, *Polym. Degrad. Stab.*, 1997, **56**, 109–113.
- Y.-F. Gao, H.-Y. Miao, H.-J. Luo and M. Nagai, *Cryst. Growth Des.*, 2008, **8**, 2187–2193.
- C.-W. Tang, C.-B. Wang and S.-H. Chien, *Thermochim. Acta*, 2008, **473**, 68–73.
- V. G. Hadjiev, M. N. Iliev and I. V. Vergilov, *J. Phys. C: Solid State Phys.*, 1988, **21**, L199.
- Y. Iida, *J. Am. Ceram. Soc.*, 1958, **41**, 397–406.
- B. Zhang, Y. Liu, Z. Huang, S. Oh, Y. Yu, Y.-W. Mai and J.-K. Kim, *J. Mater. Chem.*, 2012, **22**, 12133–12140.
- R. H. Kodama, *J. Magn. Magn. Mater.*, 1999, **200**, 359–372.
- B. Raveau and M. Seikh, *Cobalt Oxides: From Crystal Chemistry to Physics*, Wiley VCH, Weinheim, 2012.
- M. Liu, X. Shen, F. Song, J. Xiang and R. Liu, *J. Sol-Gel Sci. Technol.*, 2011, **59**, 553–560.
- M. Liu, X. Shen, F. Song, J. Xiang and X. Meng, *J. Solid State Chem.*, 2011, **184**, 871–876.
- D. Barreca, C. Massignan, S. Daolio, M. Fabrizio, C. Piccirillo, L. Armelao and E. Tondello, *Chem. Mater.*, 2001, **13**, 588–593.
- Y. Zhang, Y. Chen, T. Wang, J. Zhou and Y. Zhao, *Micropor. Mesopor. Mater.*, 2008, **114**, 257–261.
- L. J. Piliore, K. Vedam, J. E. Yehoda, R. Messier and P. J. McMarr, *Phys. Rev. B*, 1987, **35**, 9368–9371.
- I. Justicia, P. Ordejón, G. Canto, J. I. Mozos, J. Fraxedas, G. a. Battiston, R. Gerbasi and A. Figueras, *Adv. Mater.*, 2002, **14**, 1399–1402.
- D. Briggs and V. Gibson, *Chem. Phys. Lett.*, 1974, **25**, 493–496.
- E. M. Malone, S. C. Petitto and M. A. Langell, *Solid State Commun.*, 2004, **130**, 571–575.
- S. C. Petitto, E. M. Marsh, G. A. Carson and M. A. Langell, *J. Mol. Catal. A: Chem.*, 2008, **281**, 49–58.
- B. Viswanathan, S. Sivasanker and A. V. Ramaswamy, *Catalysis: Principles and Applications*, Narosa Publishing House, New Delhi, 2002.
- Zeng, J. Q. Wang, G. D. Du, W. X. Li, Z. X. Chen, S. Li, Z. P. Guo and S. X. Dou, *ArXiv e-prints*, 2012, **1207**, 3216. <http://arxiv.org/abs/1207.3216>
- Y. Sun, R. Xu, J.-Y. Yang, L. He, J.-C. Nie, R.-F. Dou, W. Zhou and L. Guo, *Nanotechnology*, 2010, **21**, 335605.